Title

Bioadsorption of Rare Earth Elements through Cell Surface Display of Lanthanide Binding Tags

Journal

Environmental Science and Technology, 50(5)

ISSN

0013-936X

Authors

Park, Dan M
Reed, David W
Yung, Mimi C
et al.

Publication Date

2016-03-01

DOI

10.1021/acs.est.5b06129

Peer reviewed

HHS Public Access

Author manuscript

Environ Sci Technol. Author manuscript; available in PMC 2017 April 05.

Published in final edited form as:

Environ Sci Technol. 2016 March 01; 50(5): 2735–2742. doi:10.1021/acs.est.5b06129.

Bioadsorption of Rare Earth Elements through Cell Surface Display of Lanthanide Binding Tags

Dan M. Park[1], **David W. Reed**[2], **Mimi C. Yung**[1], **Ali Eslamimanesh**[3], **Malgorzata M. Lencka**[3], **Andrzej Anderko**[3], **Yoshiko Fujita**[2], **Richard E. Riman**[4], **Alexandra Navrotsky**[5], and **Yongqin Jiao**[1,*]

[1]Physical and Life Science Directorate, Lawrence Livermore National Laboratory, Livermore, California 92550, United States

[2]Idaho National Laboratory, Idaho Falls, Idaho 83415, United States

[3]OLI Systems, Inc., 240 Cedar Knolls Road, Suite 301, Cedar Knolls, New Jersey 07927, United States

[4]Department of Materials Science and Engineering, Rutgers, The State University of New Jersey, 607 Taylor Road, Piscataway, New Jersey 08855, United States

[5]Peter A. Rock Thermochemistry Laboratory and NEAT ORU, University of California Davis, Davis, California 95616, United States

Abstract

With the increasing demand for rare earth elements (REEs) in many emerging clean energy technologies, there is an urgent need for the development of new approaches for efficient REE extraction and recovery. As a step towards this goal, we genetically engineered the aerobic bacterium *Caulobacter crescentus* for REE adsorption through high-density cell surface display of lanthanide binding tags (LBTs) on its S-layer. The LBT-displayed strains exhibited enhanced adsorption of REEs compared to cells lacking LBT, high specificity for REEs, and an adsorption preference for REEs with small atomic radii. Adsorbed Tb^{3+} could be effectively recovered using citrate, consistent with thermodynamic speciation calculations that predicted strong complexation of Tb^{3+} by citrate. No reduction in Tb^{3+} adsorption capacity was observed following citrate elution, enabling consecutive adsorption/desorption cycles. The LBT-displayed strain was effective for extracting REEs from the acid leachate of core samples collected at a prospective rare earth mine. Our collective results demonstrate a rapid, efficient and reversible process for REE adsorption with potential industrial application for REE enrichment and separation.

*corresponding author: Yongqin Jiao, Physical and Life Sciences Directorate, Lawrence Livermore National Laboratory, L-452, 7000 East Ave, Livermore, CA 94550, Jiao1@llnl.gov, Phone: (925) 422-4482.

Supporting Information

Sequences of LBT constructs; detailed methods for the determination of thermodynamic model parameters; Figure S1, Tb/Dy and Tb/Nd competition adsorption experiments; Figure S2, cell survival during Tb adsorption; Figure S3, predicted relative amounts of Tb species in aqueous solutions in the presence of 45 mM sodium acetate; Figure S4, relative amounts of Tb species in aqueous solution in the presence of 10 mM sodium citrate; Figure S5, competition luminescence experiments with phosphate; Table S1, primers list; Table S2, strains and plasmids list; Table S3. Sources and types of experimental data used for determining the thermodynamic model parameters.

Graphical Abstract

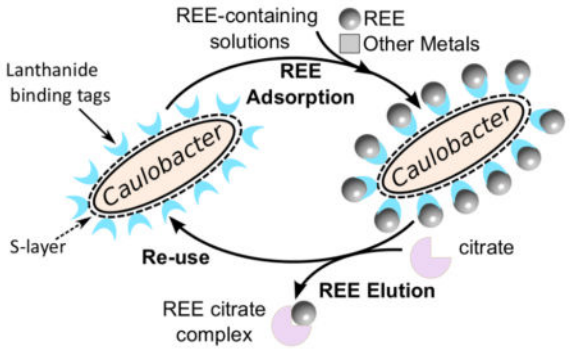

Introduction

REEs are essential components of many high-tech electronics and low-carbon technologies, including wind turbines, solar panels and hybrid/electric vehicle batteries. As such, the current uncertainty in the supply of REEs hinders the growth of several renewable energy technologies in the U.S. and Europe.[1, 2] Five REEs (Tb, Dy, Eu, Nd, and Y) in particular have been highlighted by the U.S. Department of Energy for both supply vulnerability and criticality to the development of emerging clean energy technologies.[3] Conventional REE extraction relies on energy- and/or chemical-intensive metallurgical techniques[4, 5] that can be expensive, environmentally harmful, and particularly inefficient for materials containing low concentrations of REEs. The development of low-cost and environmentally friendly approaches for ore processing/refining and recycling of REE-containing materials is crucial for achieving a sustainable balance between REE supply and demand.[1, 2]

Microbially mediated surface adsorption offers a potentially cost-effective and ecofriendly approach for metal processing. Microorganisms have long been exploited as bioadsorbents for heavy metal extraction, most notably for bioremediation.[6, 7] More recently, studies have shown significant REE adsorption capacity with various microbes,[8–12] highlighting their potential for REE extraction. However, the poor metal binding specificity of the cell wall functional groups (e.g., carboxyl and phosphoryl)[12–15] offers challenges for selective enrichment of REEs. To improve specific binding of metal ions, bioengineering approaches have been used as a cost-effective means to display selective metal-binding peptides and proteins on the cell surface.[16, 17] This approach has enabled higher capacity bioadsorption of a variety of metal ions, including Cd, Au, Pb, Mo, Hg, and uranyl ions.[18–26] In contrast, research on specific REE bioadsorption remains limited[1, 2, 8, 16] and bioengineering efforts have not been attempted for REE adsorption.

The development of lanthanide binding tags (LBTs), short peptides that have high affinity and specificity towards REEs,[27–29] has enabled the bioengineering of a REE-specific bioadsorbent. LBTs have been broadly used as REE-binding fusion proteins for biological applications, including protein purification, biosensing, NMR spectroscopy, and X-ray crystallography.[29–32] The short peptide-based nature of LBTs and high REE binding affinity make them ideal for cell surface display to increase specific REE adsorption.

The bacterium *Caulobacter crescentus* is an ideal biological system for metal adsorption due to its encapsulation by a S-layer that is highly amenable to bioengineering.[33] The S-layer protein, RsaA, is abundant with approximately 40,000 subunits per cell,[34, 35] providing a convenient anchor for high-density cell surface display of foreign proteins and peptides.[36–38] In this study, we used a bioengineering approach to display LBTs in high copy number on the S-layer of *C. crescentus*. Our results showed that the LBT-displayed cells could effectively extract REEs from REE-containing solutions.

Methods

Strain construction

The bacterial strains, plasmids, and primers used in this study are listed in the Supporting Information (Tables S1 and S2). To make p4ArsaA(723Δ)-dLBTx1, we first PCR amplified dLBT, a double lanthanide tag containing a tandem copy of sLBT3[27], using primers dLBT1 and dLBT2. Using InFusion cloning (Clontech In-Fusion HD Cloning Plus kit, Mountain View, CA), the dLBT product was inserted at amino acid position 723 of *rsaA* in the plasmid p4ArsaA(723Δ)GSCCΔ that was linearized using primers dLBT3 and dLBT4. The sequence of cloned regions was confirmed by sequencing.

The number of dLBT copies within *rsaA* was exponentially increased following the method of Nomellini et al[39]. A synthetic dsDNA fragment containing a tandem repeat of dLBT3 and the Muc1B spacer (dLBT3-muc1B-dLBT3-muc1B, Supporting information) with BglII and SpeI sites on the 5′ end and NheI and PstI sites on the 3′ end was digested with BglII and PstI and cloned into the similarly digested p4ArsaA(723Δ)GSCCΔ, yielding p4ArsaA(723Δ)-dLBTx2-Muc1B. To construct p4ArsaA(723Δ)-dLBTx4-Muc1B, the larger fragment from an NheI/HindIII digest of p4ArsaA(723Δ)-dLBTx2-Muc1B was ligated to the smaller fragment of a SpeI/HindIII digest of the same plasmid. p4ArsaA(723Δ)-dLBTx8-Muc1B was constructed by the similarly digesting and ligating p4ArsaA(723Δ)-dLBTx4-Muc1B. The dLBT-Muc1B portion of each plasmid was confirmed by sequencing and the nucleotide sequences of all constructs are provided in the Supplemental Information. Plasmids were transformed into *C. crescentus* CB2A by electroporation.

Cell growth

Caulobacter crescentus CB2A was grown at 30°C in PYE[40] with 1 μg ml^{-1} chloramphenicol. PYE was supplemented with 2.5 mM $CaCl_2$ for strain dLBTx4 and 2.5 mM $CaCl_2$ and 2 mL L^{-1} Hutner's trace metal solution[41] for strain dLBTx8. Overnight cultures were grown to late exponential phase prior to harvesting for REE adsorption assays.

Luminescence Titrations

Overnight cultures were washed once and resuspended in 10 mM MES (2-(N-morpholino)ethanesulfonic acid) buffer pH 6.1 and 10 mM NaCl to a final density of $8x10^8$ cells/ml). A Tb^{3+} stock solution (50 mM) was prepared by dissolving $TbCl_3$ hydrate salts (Sigma-Aldrich) in 100 mM HCl, and a Ca^{2+} stock solution (1 M) was prepared by dissolving $CaCl_2$ in ddH_2O. Cells were incubated with varying Tb^{3+} concentrations for 20

min prior to luminescence measurements (Ex/Em 280/544 nm)[42] using a 96-well plate reader (Biotek, CA).

For competition experiments, 50 mM stock solutions of $DyCl_3$, $EuCl_3$, $La(NO_3)_3$, Nd acetate, YCl_3, $YbCl_3$, $CeCl_3$, and $FeCl_3$ were prepared in 1 mM HCl and 50 mM stock solutions of $NiSO_4$, $ZnSO_4$, $CuSO_4$, $MnCl_2$, $MgSO_4$, $CoCl_2$, and $AlK(SO_4)_2$ were prepared in ddH_2O. Cells were initially loaded with 10 μM Tb^{3+} by incubation in Tb binding solution (10 mM MES pH 6.1, 10 mM NaCl, 10 μM $TbCl_3$) in the presence of 150 mM Ca^{2+} and luminescence was measured after 20 min. Aliquots of each metal stock were then added and luminescence was measured following a 5-min incubation. Min max normalization was used to normalize the luminescence data to the 0 – 1 range using the luminescence signal of dLBTx4 incubated with 10 μM Tb^{3+} as 1 and the luminescent signal of dLBTx4 with no Tb^{3+} as 0. Titration data were analyzed and IC_{50} values determined using the drc (dose response curve) package of R.[43] The dissociation constant (K_d) for the binding of each REE to LBTs was calculated from the IC_{50} value using the *Cheng-Prusoff equation*:[44]

$$K_d = \frac{IC_{50}}{(1+[L]/K_b)}$$

where L is the concentration of Tb^{3+} (10 μM) and K_b is the binding affinity of LBT for Tb^{3+}.

For Tb^{3+} desorption experiments, 100 mM stocks (pH 6) of sodium acetate, sodium citrate and sodium gluconate were prepared. Cells were incubated in Tb binding solution with or without 100 mM $CaCl_2$ and then subjected to various concentrations of the organic acids. Luminescence was measured after 20 min and fractional saturation was determined as described above.

Quantifying REE adsorption

REE binding experiments were performed as described above for luminescence titrations. For adsorption experiments at a pH other than 6, MES buffer was replaced with 5 mM acetate buffer (pH 5, 4.5, 4). After REE adsorption, cells were centrifuged at 20,000 x *g* for 8 min and the supernatant was extracted. Ultrapure concentrated nitric acid was used to acidify (1% v/v) the samples and the commercial standard stock solutions prior to inductively coupled plasma mass spectrometry (ICP- MS) analysis. The instrument (iCAP Q, Thermo Scientific) was standardized and operated in accordance with manufacturer's instructions. Total adsorbed REE was calculated by subtracting the REE concentration remaining in the supernatant from the concentration of REE in the control without bacterial cells.

Adsorption/desorption cycling experiments

Cells were incubated in Tb binding solution containing 150 mM $CaCl_2$ and luminescence was measured after 20 min. Citrate was added to 5 mM for 5 min before cells were centrifuged at 20,000 x *g* for 8 min. Tb^{3+} in the supernatant was quantified as described

above. The total Tb^{3+} in a solution lacking cells was used to calculate the fraction of eluted Tb^{3+}. The cell pellet was washed with 10 mM MES pH 6.1 to eliminate residual citrate, centrifuged and suspended in Tb binding solution containing 100 mM $CaCl_2$. Luminescence was measured after 5 min and normalized by the optical density at 600 nm (OD_{600}) to account for any loss in cell density during wash steps. Fractional saturation was determined as described above. Citrate elution followed by Tb^{3+} reloading was repeated twice.

REE adsorption from Bull Hill core samples

REEs from Bull Hill borehole samples (43.5 m below land surface; Rare Element Resources, Sundance, Wyoming, USA) were leached using aqua regia as follows: 300 mg of sample and 5 mL Milli-Q water were combined with 1.8 mL HCl and 700 μL of HNO_3 in a glass beaker. The beaker was covered with a watch glass and heated at 125°C for 8 h. An additional 5 mL of Milli-Q water was added and the heating step was repeated once. The total volume was adjusted to 30 mL with Milli-Q water and the pH was adjusted to 4.8. Insoluble precipitates were removed by centrifugation at 7,000 x *g* for 10 min followed by filtration using a 0.2 μm filter and soluble REEs were quantified by ICP-MS. For LBT binding reactions, the extracted REE solution was diluted 100-fold so that no individual REE exceeded 20 μM and then adjusted to pH 6 using 10 mM MES. REE concentrations in excess of the dLBTx4 binding capacity were used to determine whether there was preferential adsorption of any REE. Strain dLBTx4 and control cells were used at a density of $8x10^8$ cells/ml. Where indicated, $CaCl_2$ was added at 100 mM. After a 20 min incubation, the supernatant was collected following centrifugation as described above and Y, La, Ce and Nd, the most prevalent REE in the leachates, were quantified by ICP-MS.

Thermodynamic modeling

Equilibrium speciation calculations were performed with the previously developed Mixed-Solvent Electrolyte (MSE) thermodynamic model.[45, 46] Using the procedure described in the Supporting Information, the necessary parameters of the MSE model[45, 46] were determined to reproduce the experimental thermodynamic data for solutions containing Tb, Ca, citrates and acetates as a function of pH. The individual Tb^{3+} species present in the aqueous solution in the presence of acetate or citrate are shown in Figure S3 or Figure S4, respectively.

S-layer extraction

Assembled S layer was extracted using HEPES pH 2.0 buffer as previously described[47] and analyzed by SDS-PAGE (7%).

Results and Discussion

Genetic engineering

To effectively adsorb REEs from metal ion mixtures, we leveraged both the high affinity and selectivity of LBTs and the attractive bioengineering properties of the *C. crescentus* S-layer protein to display LBTs on the cell surface. A double LBT (hereafter dLBT) comprised of tandem sLBT3[27] was inserted into the S-layer gene, *rsaA,* yielding strain dLBTx1 (Figure 1A). Extraction and visualization of S-layer protein from strain dLBTx1 indicated that the fusion protein was displayed on the cell surface (Figure 1B).

To further improve REE adsorption capacity, the copy number of dLBT within RsaA was increased exponentially up to 8 copies, [39] resulting in strains dLBTx2, dLBTx4 and dLBTx8 (Figure 1A). Duplication of dLBT (strain dLBTx2) did not perturb S-layer formation or cell growth. However, both the dLBTx4 and dLBTx8 strains exhibited an S-layer shedding phenotype accompanied with lower growth yields (data not shown). Since calcium ions (Ca^{2+}) are known to be critical for S-layer crystallization and attachment to lipopolysaccharides on the cell wall,[48, 49] we supplemented the growth medium with additional Ca^{2+} (2.5 μM). The results showed that Ca^{2+} addition restored normal growth yield (Data not shown) and S-layer production for the dLBTx4 strain (Figure 1B). Although some improvement was observed for strain dLBTx8 with the addition of Ca^{2+} and trace metals, significant S-layer shedding still occurred, resulting in reduced S-layer production as shown by the fainter S-layer band (Figure 1B).

Terbium adsorption onto LBT-displayed cells

As one of the five REEs of highest criticality[3], Tb^{3+} adsorption onto the cell surface-displayed LBTs was first examined. Conveniently, LBTs contain a strategically placed tryptophan residue that sensitizes Tb-luminescence, allowing Tb binding to surface-displayed LBTs to be assessed through luminescence measurements. [42] As expected, strain dLBTx1 exhibited increased luminescence compared to a strain that expressed S-layer protein lacking dLBT (hereafter control strain) (Figure 2A), suggesting that surface-displayed dLBT was capable of binding Tb^{3+}. Moreover, the luminescence intensity increased with increasing number of dLBT up to four copies, suggestive of greater Tb^{3+} binding capacity. The luminescence intensity was not significantly improved in strain dLBTx8, likely due to S-layer shedding. Therefore, we chose to use strain dLBTx4 for all subsequent experiments, unless specified otherwise.

To confirm REE adsorption, suggested by luminescence measurements, we quantified Tb^{3+} adsorption using ICP-MS. Initial measurements showed similar Tb^{3+} adsorption between dLBTx4 and the control strain at all Tb^{3+} concentrations tested (Figure 2B). Both strains adsorbed up to ~$6.25x10^{-8}$ nmole Tb^{3+} per cell, equating to 50 μM of Tb^{3+} at a cell concentration of $8x10^{8}$ cells per mL. A variety of other bacteria and algae species including *E. coli, Bacillus subtilis,* and *Pseudomonas* species have been reported to adsorb REEs (e.g., Eu, Yb and Dy), with adsorption ranging from 1–100 μM at similar cell concentrations.[8–12, 17, 50] The adsorption of rare earth ions by these native microbial systems is mediated by the presence of functional groups (e.g., phosphates and carboxyls) on the cell wall as well as through the cellular release of inorganic phosphate.[6, 12] Although the background cell wall adsorption of Tb^{3+} may serve to further increase the REE binding capacity, it is unlikely to possess the same level of specificity for REE that is characteristic of LBTs. As such, cell wall adsorption is likely undesirable for the purpose of REE enrichment.

To mitigate the background ion adsorption, we added Ca^{2+} as a competitor. Rare earth ions and Ca^{2+} have a similar ionic radius and oxophilicity[51] and a previous report suggested that excess Ca^{2+} blocks the formation of Tb^{3+} deposits on the bacterial membrane.[52] Furthermore, Ca is a common metal present in REE-containing source materials.[53] With 100

mM Ca^{2+}, although overall Tb^{3+} adsorption ($2.6x10^{-8}$ nmole/cell capacity for dLBTx4) was lower compared to conditions with no added Ca^{2+}, dLBTx4 adsorbed a significantly greater amount of Tb^{3+} compared to the control at all tested Tb^{3+} concentrations (Figure 2C and 2E). This suggested that while the vast majority of non-LBT sites on the cell wall were occupied by Ca^{2+}, the REE-selective LBT sites were still available for Tb^{3+} binding. Consequently, a significant increase in apparent binding affinity of LBT for Tb^{3+} was observed in all engineered strains (Figure 2D). Higher Ca^{2+} concentrations beyond ~100 mM did not further decrease background cell wall binding (Figure 2E), and thus, 100–150 mM Ca^{2+} was used in the subsequent metal adsorption experiments described below. The absence of a Ca^{2+} effect on Tb^{3+} adsorption by dLBTx4 in Figure 2E is indicative of excess LBT relative to added Tb^{3+} (10 μM); Figure 2C suggests that at the cell concentrations used in these assays, surface displayed LBT can adsorb 12.9 ± 4.6 μM Tb^{3+}.

Given the poor solubility of REEs at neutral and alkaline pH and the fact that REE-containing aqueous solutions during REE processing tend to be acidic,[1, 4] we evaluated REE adsorption within the pH range of 4–6 (Figure 2F). Tb^{3+} adsorption to dLBTx4 was maximal at pH 6 (93% of Tb added), reduced to ~60% at pH 5 and to ~40% at pH 4.5 and 4. Minimal adsorption was observed below pH 4 as evidenced by luminescence measurements (data not shown). Thus, LBT-displayed cells are most effective in a pH range of 5–6.

REE adsorption specificity

Since REE sources frequently coexist with other metal contaminants in both ores and recycled materials,[54] we evaluated Tb^{3+} adsorption in the presence of various metal ions. Competition experiments were performed by loading LBTx4 cells with Tb^{3+} followed by monitoring the decrease in luminescence intensity in response to increasing concentrations of other metal ions (Figure 3A). LBTx4 displayed high selectivity for Tb^{3+} over other metal ions tested. With the exception of Cu^{2+}, addition of metal ions up to at least 100 μM, an order of magnitude higher than the Tb^{3+} concentration, had minimal effect on Tb^{3+} binding. Given that Cu^{2+} was the most effective competitor based on luminescence, Tb^{3+} adsorption was quantified by ICP-MS in the presence of Cu^{2+} (Figure 3B). In agreement with the luminescence data, higher Cu^{2+} concentrations (1 mM) were inhibitory for Tb^{3+} adsorption. However, the results observed with 100 μM Cu^{2+} were inconsistent between the two measurement methods: nearly 100% Tb^{3+} adsorption was measured by ICP-MS, whereas a 60% reduction in luminescence was observed, which could be due to luminescence quenching by Cu^{2+}.[55] Overall, the weak affinity of surface displayed LBTs for non REE metal ions suggests that REE adsorption is largely unaffected by the presence of commonly occurring metal ions in source materials, at least at concentrations up to 100-fold higher than REEs.

We also conducted experiments to determine adsorption selectivity among REEs. Due to their similar physiochemical properties, it is very difficult to chemically separate REEs from one another, often requiring dozens of organic solvent extraction steps.[4] Competition binding experiments revealed that dLBTx4 preferred REEs with smaller atomic radii (Figure 3C; Table 1), similar to results with LBT peptides in solution.[42] Eu^{3+}, Dy^{3+} and Yb^{3+} were all effective competitors of Tb^{3+}, with binding affinities of ~3 μM, whereas Y^{3+} and Nd^{3+}

were slightly poorer competitors. La^{3+} and Ce^{3+}, with the largest atomic radii among REEs, were the weakest substrates for LBT. Consistent with this data, ICP-MS measurements of REE adsorption in the presence of equimolar Tb^{3+}/Dy^{3+} or Tb^{3+}/Nd^{3+} mixtures revealed no significant preference for one REE over the other (Figure S1). In contrast, Tb^{3+} was preferentially adsorbed over La^{3+} when both REEs were present in equimolar concentrations (Figure 3D). Overall, our results suggest that the LBT-displayed strains have the potential to selectively enrich for REEs with smaller radii, including all five REEs of high criticality. This is an important feature given the high relative abundance of La and Ce in many REE source materials.[54]

REE desorption

Since the ability to reuse the engineered cells for metal adsorption would lower the cost associated with cell regeneration for industrial applications, we examined REE desorption and subsequent re-adsorption (recycling) and established a general strategy for REE recovery. A variety of chemicals including acids, salts and ligands have been used for metal desorption from environmental surfaces.[50] In particular, some organic acids such as citric acid are able to form strong complexes with REEs.[56] We found that Tb^{3+} was fully recovered from the dLBTx4 cell surface with l–5 mM citrate (Figure 4A). In contrast, acetate or gluconate were much less effective, even at much higher concentration (45 mM; Figure 4A). A higher concentration of organic acids was required when Ca^{2+} was present in the reaction mixture, presumably due to complexation of the organic acids with Ca^{2+} (see discussion in paragraph below). Importantly, the REE adsorption capacity is fully maintained over at least two rounds of citrate-mediated desorption (Figure 4B). Furthermore, cell viability was not significantly affected by Tb^{3+} adsorption (Figure S2), suggesting that Tb^{3+} is not toxic on the timescale of adsorption experiments. The rapid and reversible nature of REE-cell binding should facilitate efficient recovery of REEs, alleviating the need for cell regeneration between extraction rounds.

Thermodynamic speciation analysis based on the Mixed-Solvent Electrolyte (MSE) thermodynamic model[45, 46] was used to quantitatively rationalize Tb^{3+} desorption by the organic acids. If the desorption of Tb^{3+} is attributed to the complexation with organic acids in solution, the amount of Tb^{3+} desorbed should be proportional to Tb^{3+} complexed in solution. As expected, the predicted fraction of uncomplexed Tb^{3+} decreased with increasing organic acid concentration (Figure 4C, D), corresponding with the observed decrease in the fraction of Tb^{3+} bound to dLBTx4 (Figure 4A). It is also evident that citrate is a much stronger complexant of Tb^{3+} than acetate (Figures 4C and 4D). Specifically, complexation of Tb^{3+} with citrate is predicted to occur over a narrow range of citrate concentrations with 10 μM sufficient to complex almost all Tb^{3+}. In contrast, more than 45 mM acetate was predicted to be required to complex the majority of Tb^{3+} and only at high pH (cf. pH=6.1 in Figure 4C). Additionally, the predicted complex formation between Ca^{2+} and acetate or citrate explains, at least in part, the requirement for greater concentrations of these organic acids for Tb^{3+} desorption in the presence of Ca^{2+}, as shown in Figure 4A. This Ca^{2+} effect on desorption can also be attributed to the increased apparent binding affinity of LBT for Tb^{3+} in the presence of Ca^{2+} (Figure 2D).

REE adsorption from sediment core samples

As a preliminary step towards application, we tested REE adsorption from the acid leachate of core samples collected from the Bull Hill Mine. The high relative abundance of Nd, a REE of high criticality, and the low phosphate concentrations are attractive features for bioadsorption at near neutral pH. We found that phosphate reduced REE adsorption capacity (Figure S5), likely due to the formation of insoluble REE phosphate phases.[57, 58] For the predominant four REEs in the leachate (Y, La, Ce, Nd), dLBTx4 outperformed the control cells, even without exogenous Ca^{2+} supplementation (Table 2). As expected, although the total amount of the REE adsorption decreased with Ca^{2+} addition, the relative disparity in adsorption between dLBTx4 and control cells was enhanced by 100 mM Ca^{2+} addition (Table 2), consistent with reduced REE binding to the cell wall (Figure 2C). Furthermore, as expected, dLBTx4 cells exhibited preferential adsorption of Nd^{3+}, Y^{3+} and Ce^{3+} over La^{3+} (apparent in presence of excess Ca^{2+}; Table 2). Together, these data demonstrate the utility of LBT-displayed cells for REE extraction from minimally processed source materials.

We envision that the scalable and reusable bioadsorption platform for selective extraction of REEs developed in this study may prove particularly useful for REE extraction from waste streams with relatively low REE content (e.g., ore tailing, bauxite mine residues, phosphogypsum, incinerator ash, metallurgy slags, acid mine drainage, and industrial and municipal wastewaters).[1, 2, 54 50] Following a minimal solution conditioning (i.e., pH adjustment and potentially Ca^{2+} addition), rapid, and reversible REE adsorption by LBT-displayed strains could enable a low cost and environmentally friendly alternative for REE extraction and processing.

Supplementary Material

Refer to Web version on PubMed Central for supplementary material.

Acknowledgments

We thank Adrian Van Rythoven at Rare Earth Resources for providing sediment core samples from Bull Hill. This research is supported by the Critical Materials Institute, an Energy Innovation Hub funded by the U.S. Department of Energy, Office of Energy Efficiency and Renewable Energy, Advanced Manufacturing Office. This work was performed under the auspices of the U.S. Department of Energy by Lawrence Livermore National Laboratory under Contract DEAC52-07NA27344 (LLNL-JRNL-679871) and by Idaho National Laboratory under DOE Idaho Operations Office Contract DE-AC07-05ID14517.

References

1. Zhuang WQ, Fitts JP, Ajo-Franklin CM, Maes S, Alvarez-Cohen L, Hennebel T. Recovery of critical metals using biometallurgy. Curr Opin Biotechnol. 2015; 33:327–335. [PubMed: 25912797]
2. Hennebel T, Boon N, Maes S, Lenz M. Biotechnologies for critical raw material recovery from primary and secondary sources: R&D priorities and future perspectives. New biotechnology. 2015; 32(1):121–7. [PubMed: 23994422]
3. DOE. Critical Materials Strategy. 2011. http://www.energy.gov
4. Xie F, Zhang TA, Dreisinger D, Doyle F. A critical review on solvent extraction of rare earths from aqueous solutions. Miner Eng. 2014; 56:10–28.
5. Nash KL, Jensen MP. Analytical-scale separations of the lanthanides: A review of techniques and fundamentals. Separ Sci Technol. 2001; 36(5–6):1257–1282.

6. Gadd GM. Metals, minerals and microbes: geomicrobiology and bioremediation. Microbiology. 2010; 156(Pt 3):609–43. [PubMed: 20019082]
7. Blackwell KJ, Singleton I, Tobin JM. Metal cation uptake by yeast: a review. Appl Microbiol Biotechnol. 1995; 43(4):579–84. [PubMed: 7546600]
8. Moriwaki H, Yamamoto H. Interactions of microorganisms with rare earth ions and their utilization for separation and environmental technology. Appl Microbiol Biotechnol. 2013; 97(1):1–8. [PubMed: 23111596]
9. Texier AC, Andres Y, Le Cloirec P. Selective biosorption of lanthanide (La, Eu, Yb) ions by *Pseudomonas aeruginosa*. Environ Sci Technol. 1999; 33(3):489–495.
10. Tsuruta T. Accumulation of rare earth elements in various microorganisms. J Rare Earth. 2007; 25(5):526–532.
11. Ozaki T, Gillow JB, Kimura T, Ohnuki T, Yoshida Z, Francis AJ. Sorption behavior of europium(III) and curium(III) on the cell surfaces of microorganisms. Radiochim Acta. 2004; 92(9–11):741–748.
12. Jiang MY, Ohnuki T, Tanaka K, Kozai N, Kamiishi E, Utsunomiya S. Post-adsorption process of Yb phosphate nano-particle formation by *Saccharomyces cerevisiae*. Geochim Cosmochim Ac. 2012; 93:30–46.
13. Fein JB, Martin AM, Wightman PG. Metal adsorption onto bacterial surfaces: Development of a predictive approach. Geochim Cosmochim Ac. 2001; 65(23):4267–4273.
14. Ginn BR, Fein JB. The effect of species diversity on metal adsorption onto bacteria. Geochim Cosmochim Ac. 2008; 72(16):3939–3948.
15. Naeem A, Woertz JR, Fein JB. Experimental measurement of proton, Cd, Pb, Sr, and Zn adsorption onto the fungal species *Saccharomyces cerevisiae*. Environ Sci Technol. 2006; 40(18):5724–5729. [PubMed: 17007132]
16. Mejare M, Bulow L. Metal-binding proteins and peptides in bioremediation and phytoremediation of heavy metals. Trends Biotechnol. 2001; 19(2):67–73. [PubMed: 11164556]
17. Kuroda K, Ueda M. Engineering of microorganisms towards recovery of rare metal ions. Appl Microbiol Biotechnol. 2010; 87(1):53–60. [PubMed: 20393699]
18. Kotrba P, Doleckova L, De Lorenzo V, Ruml T. Enhanced bioaccumulation of heavy metal ions by bacterial cells due to surface display of short metal binding peptides. Appl Environ Microbiol. 1999; 65(3):1092–1098. [PubMed: 10049868]
19. Wei W, Liu X, Sun P, Wang X, Zhu H, Hong M, Mao ZW, Zhao J. Simple Whole-Cell Biodetection and Bioremediation of Heavy Metals Based on an Engineered Lead-Specific Operon. Environ Sci Technol. 2014; 48(6):3363–3371. [PubMed: 24564581]
20. Wei W, Zhu TZ, Wang Y, Yang HL, Hao ZY, Chen PR, Zhao J. Engineering a gold-specific regulon for cell-based visual detection and recovery of gold. Chem Sci. 2012; 3(6):1780–1784.
21. Nishitani T, Shimada M, Kuroda K, Ueda M. Molecular design of yeast cell surface for adsorption and recovery of molybdenum, one of rare metals. Appl Microbiol Biotechnol. 2010; 86(2):641–8. [PubMed: 19894045]
22. Xu Z, Lei Y, Patel J. Bioremediation of soluble heavy metals with recombinant Caulobacter crescentus. Bioeng Bugs. 2010; 1(3):207–12. [PubMed: 21326927]
23. Zhou L, Bosscher M, Zhang C, Ozcubukcu S, Zhang L, Zhang W, Li CJ, Liu J, Jensen MP, Lai L, He C. A protein engineered to bind uranyl selectively and with femtomolar affinity. Nature chemistry. 2014; 6(3):236–41.
24. Valls M, de Lorenzo V, Gonzalez-Duarte R, Atrian S. Engineering outer-membrane proteins in *Pseudomonas putida* for enhanced heavy-metal bioadsorption. J Inorg Biochem. 2000; 79(1–4): 219–223. [PubMed: 10830869]
25. Mauro JM, Pazirandeh M. Construction and expression of functional multi-domain polypeptides in *Escherichia coli*: expression of the Neurospora crassa metallothionein gene. Lett Appl Microbiol. 2000; 30(2):161–6. [PubMed: 10736021]
26. Pazirandeh M, Wells BM, Ryan RL. Development of bacterium-based heavy metal biosorbents: enhanced uptake of cadmium and mercury by *Escherichia coli* expressing a metal binding motif. Appl Environ Microbiol. 1998; 64(10):4068–72. [PubMed: 9758845]

27. Martin LJ, Hahnke MJ, Nitz M, Wohnert J, Silvaggi NR, Allen KN, Schwalbe H, Imperiali B. Double-lanthanide-binding tags: Design, photophysical properties, and NMR applications. J Am Chem Soc. 2007; 129(22):7106–7113. [PubMed: 17497862]
28. Nitz M, Franz KJ, Maglathlin RL, Imperiali B. A powerful combinatorial screen to identify high-affinity terbium(III)-binding peptides. Chembiochem. 2003; 4(4):272–6. [PubMed: 12672106]
29. Liang HH, Deng X, Bosscher M, Ji QJ, Jensen MP, He C. Engineering Bacterial Two-Component System PmrA/PmrB to Sense Lanthanide Ions. J Am Chem Soc. 2013; 135(6):2037–2039. [PubMed: 23350529]
30. Allen KN, Imperiali B. Lanthanide-tagged proteins--an illuminating partnership. Curr Opin Chem Biol. 2010; 14(2):247–54. [PubMed: 20102793]
31. Franz KJ, Nitz M, Imperiali B. Lanthanide-binding tags as versatile protein coexpression probes. Chembiochem. 2003; 4(4):265–271. [PubMed: 12672105]
32. Silvaggi NR, Martin LJ, Schwalbe H, Imperiali B, Allen KN. Double-lanthanide-binding tags for macromolecular crystallographic structure determination. J Am Chem Soc. 2007; 129(22):7114–7120. [PubMed: 17497863]
33. Amat F, Comolli LR, Nomellini JF, Moussavi F, Downing KH, Smit J, Horowitz M. Analysis of the Intact Surface Layer of *Caulobacter crescentus* by Cryo-Electron Tomography. J Bacteriol. 2010; 192(22):5855–5865. [PubMed: 20833802]
34. Nomellini JF, Li C, Lavallee D, Shanina I, Cavacini LA, Horwitz MS, Smit J. Development of an HIV-1 specific microbicide using *Caulobacter crescentus* S-layer mediated display of CD4 and MIP1alpha. PLoS One. 2010; 5(4):e10366. [PubMed: 20442778]
35. Ford MJ, Nomellini JF, Smit J. S-layer anchoring and localization of an S-layer-associated protease in *Caulobacter crescentus*. J Bacteriol. 2007; 189(6):2226–37. [PubMed: 17209028]
36. Bingle WH, Nomellini JF, Smit J. Linker mutagenesis of the *Caulobacter crescentus* S-layer protein: Toward a definition of an N-terminal anchoring region and a C-terminal secretion signal and the potential for heterologous protein secretion. J Bacteriol. 1997; 179(3):601–611. [PubMed: 9006010]
37. Farr C, Nomellini JF, Ailon E, Shanina I, Sangsari S, Cavacini LA, Smit J, Horwitz MS. Development of an HIV-1 Microbicide Based on *Caulobacter crescentus*: Blocking Infection by High-Density Display of Virus Entry Inhibitors. PLoS One. 2013; 8(6):e65965. [PubMed: 23840383]
38. Duval M, Lewis CJ, Nomellini JF, Horwitz MS, Smit J, Cavacini LA. Enhanced neutralization of HIV by antibodies displayed on the S-layer of *Caulobacter crescentus*. Antimicrob Agents Chemother. 2011; 55(12):5547–52. [PubMed: 21896905]
39. Nomellini JF, Duncan G, Dorocicz IR, Smit J. S-layer-mediated display of the immunoglobulin G-binding domain of streptococcal protein G on the surface of *Caulobacter crescentus*: Development of an immunoactive reagent. Appl Environ Microbiol. 2007; 73(10):3245–3253. [PubMed: 17384306]
40. Park DM, Jiao Y. Modulation of medium pH by *Caulobacter crescentus* facilitates recovery from uranium-induced growth arrest. Appl Environ Microbiol. 2014; 80(18):5680–8. [PubMed: 25002429]
41. Hutner SH, Provasoli L, Shatz A, Haskins CP. Some approaches to the study of the role of metals in the metabolism of microorganisms. Proc Am Philos Soc. 1950; 94:152–170.
42. Nitz M, Sherawat M, Franz KJ, Peisach E, Allen KN, Imperiali B. Structural origin of the high affinity of a chemically evolved lanthanide-binding peptide. Angew Chem Int Edit. 2004; 43(28): 3682–3685.
43. Ritz C, Streibig JC. Bioassay analysis using R. J Stat Softw. 2005; 12(5):1–22.
44. Cheng Y, Prusoff WH. Relationship between the inhibition constant (K1) and the concentration of inhibitor which causes 50 per cent inhibition (150) of an enzymatic reaction. Biochemical pharmacology. 1973; 22(23):3099–108. [PubMed: 4202581]
45. Wang P, Anderko A, Springer RD, Young RD. Modeling Phase Equilibria and Speciation in Mixed-Solvent Electrolyte Systems: II. Liquid-Liquid Equilibria and Properties of Associating Electrolyte Solutions. Journal of Molecular Liquids. 2006; 125(1):37–44.

46. Wang P, Anderko A, Young RD. A Speciation-Based Model for Mixed-Solvent Electrolyte Systems. Fluid Phase Equilibria. 2002; 203(1–2):141–176.
47. Walker SG, Smith SH, Smit J. Isolation and comparison of the paracrystalline surface layer proteins of freshwater caulobacters. J Bacteriol. 1992; 174(6):1783–92. [PubMed: 1548228]
48. Smit J, Engelhardt H, Volker S, Smith SH, Baumeister W. The S-layer of *Caulobacter crescentus*: three-dimensional image reconstruction and structure analysis by electron microscopy. J Bacteriol. 1992; 174(20):6527–38. [PubMed: 1400205]
49. Nomellini JF, Kupcu S, Sleytr UB, Smit J. Factors controlling in vitro recrystallization of the *Caulobacter crescentus* paracrystalline S-layer. J Bacteriol. 1997; 179(20):6349–54. [PubMed: 9335282]
50. Lo YC, Cheng CL, Han YL, Chen BY, Chang JS. Recovery of high-value metals from geothermal sites by biosorption and bioaccumulation. Bioresour Technol. 2014; 160:182–190. [PubMed: 24581863]
51. Bunzli JC. Benefiting from the unique properties of lanthanide ions. Accounts of chemical research. 2006; 39(1):53–61. [PubMed: 16411740]
52. Bayer ME, Bayer MH. Lanthanide accumulation in the periplasmic space of Escherichia coli B. J Bacteriol. 1991; 173(1):141–9. [PubMed: 1987113]
53. Jones, AP., Wall, F., Williams, CT. Rare Earth Minerals: chemistry origin and ore deposits. Chapman & Hall; 1996.
54. Binnemans K, Jones PT, Blanpain B, Van Gerven T, Yang YX, Walton A, Buchert M. Recycling of rare earths: a critical review. Journal of Cleaner Production. 2013; 51:1–22.
55. Rahimi Y, Goulding A, Shrestha S, Mirpuri S, Deo SK. Mechanism of copper induced fluorescence quenching of red fluorescent protein, DsRed. Biochem Bioph Res Co. 2008; 370(1): 57–61.
56. Goyne KW, Brantley SL, Chorover J. Rare earth element release from phosphate minerals in the presence of organic acids. Chem Geol. 2010; 278(1–2):1–14.
57. Firsching FH, Brune SN. Solubility Products of the Trivalent Rare-Earth Phosphates. J Chem Eng Data. 1991; 36(1):93–95.
58. Fujita Y, Barnes J, Eslamimanesh A, Lencka MM, Anderko A, Riman RE, Navrotsky A. Effects of Simulated Rare Earth Recycling Wastewaters on Biological Nitrification. Environ Sci Technol. 2015; 49(16):9460–8. [PubMed: 26132866]

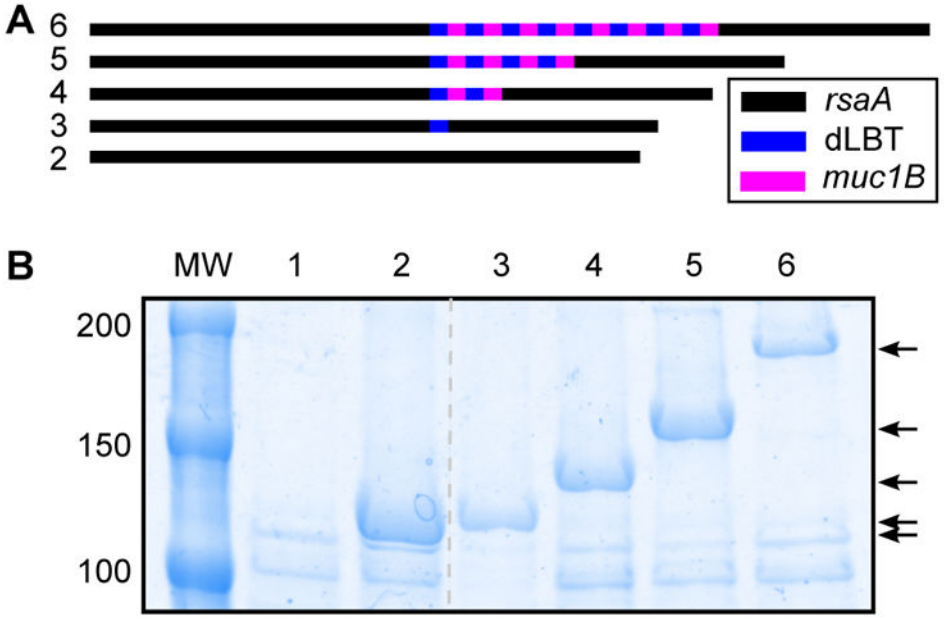

Figure 1. Bioengineering of *Caulobacter crescentus* for REE adsorption

(A). Diagram of engineered S-layer gene (*rsaA*) constructs with dLBT insertions. A muc1B spacer, encoding the human mucin protein, was appended to the C-terminal end of dLBT. The copy number of the resulting dLBT-mucR1 peptide was increased exponentially. The number labels of the constructs correspond to the lanes described in (B). (B) SDS-PAGE of S-layer extracted from the following strains: 1) wild type CB2A, 2) CB2A rsaA (control), 3) dLBTx1, 4) dLBTx2, 5) dLBTx4 and 6) dLBTx8. dLBTx4 and dLBTx8 cells were grown in PYE medium supplemented with additional Ca^{2+} (2.5 μM) and Ca^{2+} (2.5 μM) with trace metals, respectively. MW; molecular weight (kDa) markers. Arrows on the right indicate the engineered RsaA protein expressed from each strain.

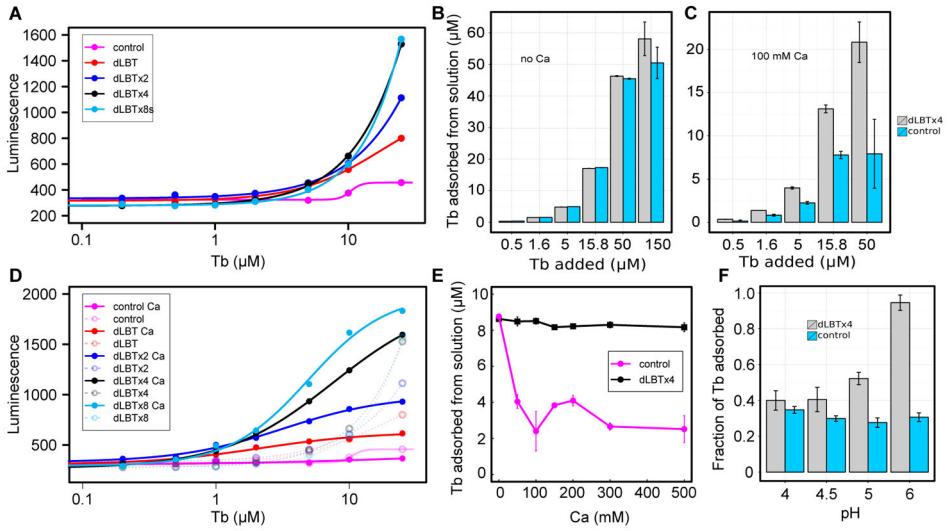

Figure 2. Tb^{3+} adsorption to LBT-displayed cells

(A) Tb^{3+} titration of dLBT constructs with no added Ca^{2+}, measured by luminescence (ex/em 280/544). ICP-MS quantitation of Tb^{3+} adsorption by dLBTx4 and control cells at increasing Tb^{3+} concentration in the absence (B) or presence (C) of 100 mM Ca^{2+}. The adsorption contribution of LBT in dLBTx4 was approximated by subtracting the total adsorbed Tb^{3+} by the control strain from that adsorbed by dLBTx4, yielding 12.9 ± 4.6 μM Tb^{3+}. The uncertainty in this expression was determined using error propagation. (D) Tb^{3+} titration of dLBT constructs with 100 mM Ca^{2+}. The data from (A) were plotted as dotted lines for comparison. (E) ICP-MS quantitation of Tb^{3+} (10 μM added) adsorption by dLBTx4 and control cells at different Ca^{2+} concentrations. (F) ICP-MS quantitation of Tb^{3+} (10 μM added) adsorption by dLBTx4 and control cells within the pH range of 4–6 in the presence of 100 mM Ca^{2+}.

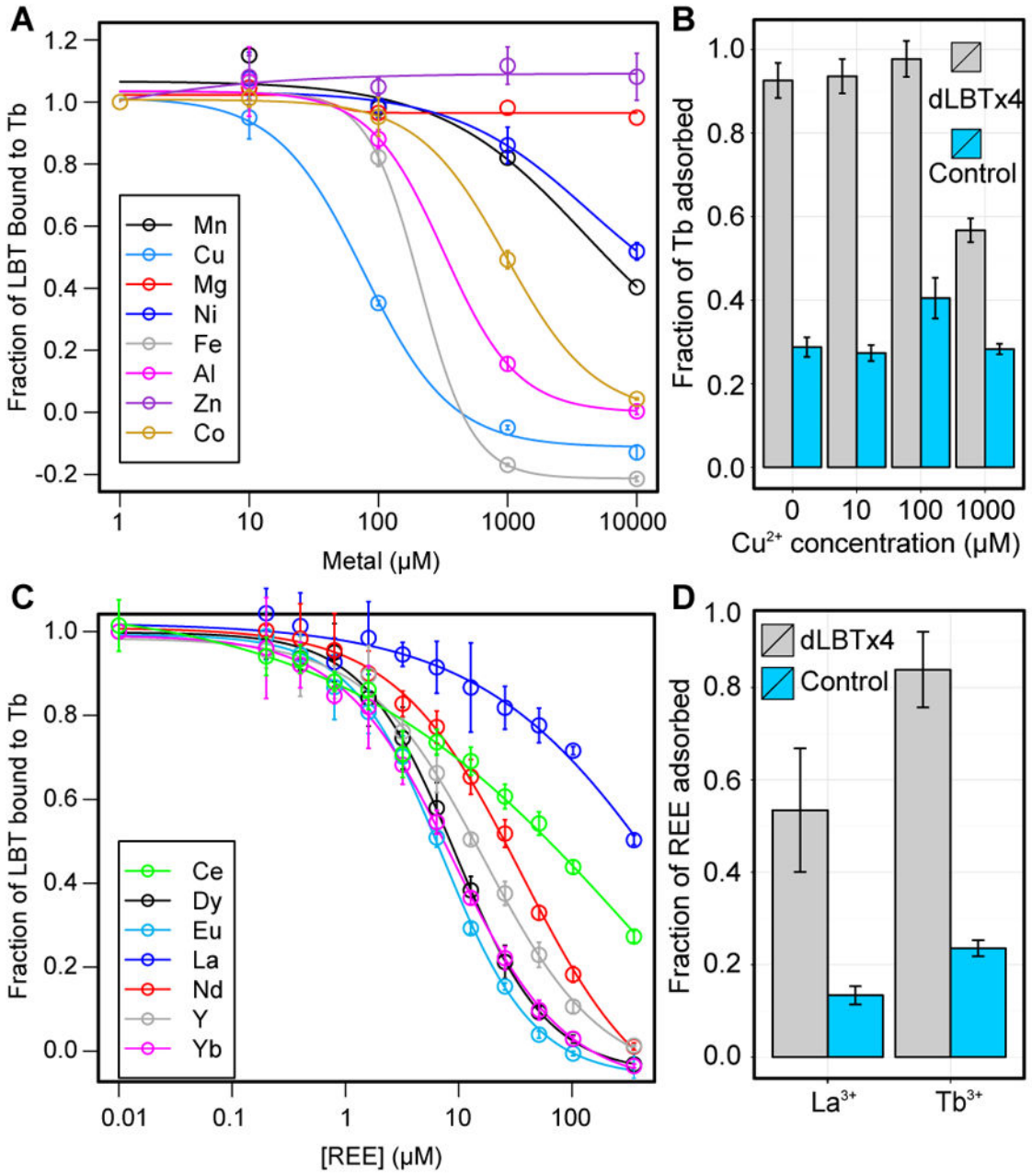

Figure 3. REE adsorption specificity

(A) Competition binding experiments with dLBTx4 cells preloaded with 10 μM Tb^{3+} followed by addition of various metal ions at concentrations up to 10 mM. Normalized luminescence was calculated as described in methods. (B) Tb^{3+} adsorption to dLBTx4 and control cells at increasing Cu^{2+} concentrations. The fraction of Tb^{3+} adsorbed was determined by quantifying the soluble Tb^{3+} concentrations before and after incubation with cells using ICP-MS. (C) Competition experiments with dLBTx4 cells preloaded with 10 μM Tb^{3+} followed by addition of REE ions up to 352 μM. Normalized luminescence was calculated as described in methods. (D) Tb^{3+} and La^{3+} (20 μM each) adsorption to dLBTx4 and control cells. The fraction of REE bound was determined by ICP-MS. All experiments

were performed in the presence of 150 mM Ca^{2+}. Error bars represent standard deviations of three replicates.

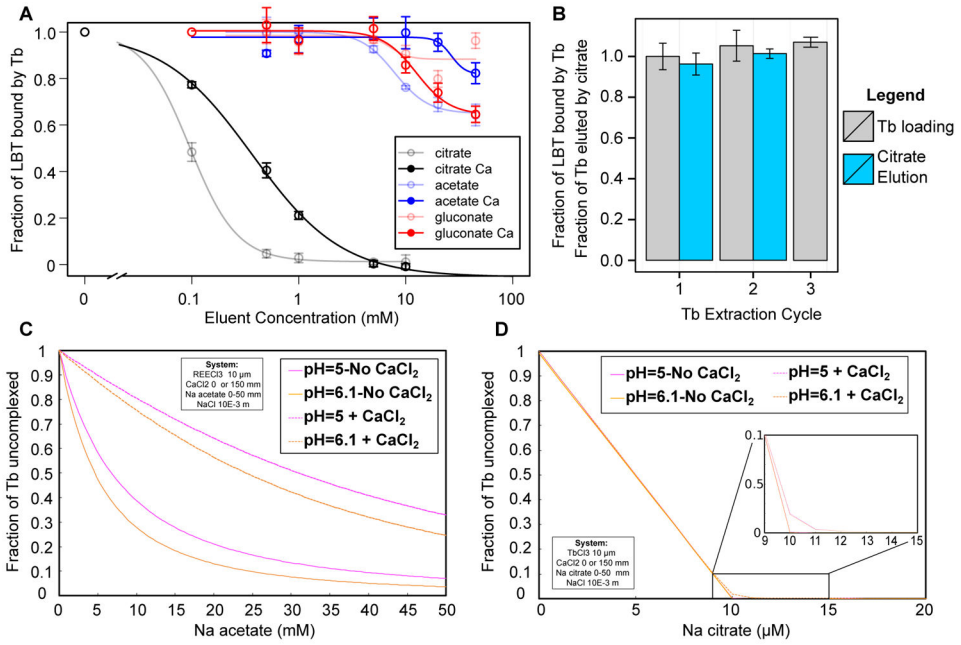

Figure 4. Citrate-mediated REE desorption

(A) REE desorption and recovery were performed by pre-loading dLBTx4 cells with 10 μM Tb^{3+} in the presence or absence of 150 mM Ca^{2+} followed by the addition of increasing concentrations of citrate, gluconate or acetate. Normalized luminescence was calculated as described in methods. (B) Three cycles of Tb^{3+} adsorption and desorption were performed with citrate (5 mM) in the presence of 150 mM Ca^{2+}. Gray bars depict the normalized luminescence signal for Tb^{3+} loading and blue bars depict the fraction of Tb^{3+} eluted using 5 mM citrate during each cycle as quantified by ICP-MS. (C) and (D) The predicted fraction of Tb^{3+} that was not complexed with acetate or citrate, respectively, using the thermodynamic model. Results are shown for pH 5 and 6.1 within the range of acetate and citrate concentrations used in (A). Note that the concentration scale in Fig. 4D is expanded to focus on the rapid decline in uncomplexed Tb at low citrate concentrations. The individual Tb^{3+} species present in the aqueous solution in the presence of acetate or citrate are shown in Figure S3 or Figure S4, respectively.

Table 1

REE specificity of strain dLBTx4.

REE	KD (μM)
Eu	2.5 (0.2)[a]
Yb	3.1 (0.3)
Dy	3.2 (0.7)
Tb	3.8 (0.3)
Y	5.7 (0.1)
Nd	13.3 (3.8)
Ce	114 (53)
La	153 (55)

[a]numbers in () represent standard deviations of 3 replicates.

Table 2

REE adsorbed from the acid leachate of soil samples from the Bull Hill Mine.

Sample	Y (μM)	La (μM)	Ce (μM)	Nd (μM)
Bull Hill leachate[a]	1.1 (0.1)[b]	15.9 (1.2)	19.4 (2.1)	15.3 (1.7)
Control	0.4 (0.0)	5.8 (1.05)	9.4 (0.3)	7.8 (0.2)
dLBTx4	0.8 (0.0)	10.9 (0.4)	14.7 (0.3)	12.1 (0.2)
Control +100 mM CaCl2	0.1 (0.0)	1.3 (0.1)	3.5 (0.1)	3.0 (0.2)
dLBTx4 +100 mM CaCl2	0.4 (0.0)	3.5 (0.6)	7.7 (0.9)	6.7 (0.7)

[a] Soluble REE concentrations after acid dissolution and pH adjustment to 6.0

[b] numbers in () represent standard deviations of 3 replicates.